Available online at www.sciencedirect.com

jmr&t Journal of Materials Research and Technology

journal homepage: www.elsevier.com/locate/jmrt

Effect of scandium on grain refinement mechanism and mechanical properties of Al–7Si–0.6 Mg alloy at different cooling rates

Hongkui Mao [a,*], *Peng Lian* [a], *Qi Wei* [a], *Yu Wang* [a], *Hong Xu* [a], *Yanjun Li* [b,**]

[a] *School of materials Science and engineering, North University of China, Taiyuan, Shanxi, China*
[b] *Department of Materials Science and Engineering, Norwegian University of Science and Technology, 7491, Trondheim, Norway*

ARTICLE INFO

Article history:
Received 31 May 2023
Accepted 23 August 2023
Available online 26 August 2023

Keywords:
Cooling rate
Grain refinement
$(Al, Si)_3(Ti, Sc)$
Modification

ABSTRACT

The effects of scandium (Sc) additions on the solidification microstructure and mechanical properties of Al–7Si–0.6Mg-0.25Ti alloy at different cooling rates have been systematically studied by thermal analysis and detailed SEM and TEM microstructure characterization of the castings. It is found that the addition of Sc has significant effects of refining the grain structure and modifying the Al–Si eutectics into fibrous structure. As a result, substantially improved strength and ductility in the as-cast state have been achieved in the Sc-added alloy. More importantly, the addition of Sc reduces the sensitivity of the alloy's strength and ductility to local cooling rates in the castings. The underlying mechanisms on the grain refinement, modification of Al–Si eutectics and strengthening by Sc addition have been studied. A new phase, DO_{22} structured $(Al, Si)_3(Ti, Sc)$, has been found to form in the liquid aluminium, acting as high potency nucleation sites of Al grains, which overcomes the Si poisoning effect on grain refinement for Al–Ti–B grain refiners.

1. Introduction

Al–Si–Mg based foundry alloys, such as A356, A357, are widely used in automotive, aerospace and other engineering applications because of their good mechanical properties, excellent casting properties, high wear resistance and low cost [1–3]. However, in the casting process, the coarse plate shaped eutectic Si forming during solidification significantly reduces the toughness of Al–Si–Mg alloys [4,5]. In order to improve the toughness of Al–Si–Mg alloys, the size and morphology of Al–Si eutectics have to be modified [6]. Addition of strontium (Sr) is one of the mostly used methods to modify the morphology of Al–Si eutectics, from coarse lamellar shaped to fine fibrous structure. The underlying modification mechanism has been extensively studied in the last decades. It is found that Sr has the influence of changing the growth mechanism by enhancing the twinning of eutectic Si phases, which is so-called impurity-induced twinning (IIT) mechanism [7]. The IIT mechanism has been realized by the preferential adsorption of Sr atoms at the twin plane re-entrant corners of Si particles, poisoning the attachment sites of Si atoms and hindering the plate growth. Another influence of Sr is to react with P in the aluminium melt to reduce

* Corresponding author.
** Corresponding author.
E-mail addresses: maohk@nuc.edu.cn (H. Mao), yanjun.li@ntnu.no (Y. Li).
https://doi.org/10.1016/j.jmrt.2023.08.227

the potent nucleation sites of Si particles, AlP. As a result, Al–Si eutectics have to nucleate and grow under a larger undercooling. This effect has been revealed by Mathiesen et al. [8] by using in-situ synchrotron X-ray radiography study in an Al–Si–Cu alloy, where the change of the eutectic Si from needle-like to fibrous morphology by Sr addition is observed. However, modification by Sr has the disadvantage of causing serious porosity problem in castings [9,10].

Another important method to improve the mechanical properties of Al–Si–Mg foundry alloys is to refine the solidification grain structure by inoculation. Al–Ti–B master alloys are widely used for grain refinement [11–14] of aluminium alloys. However, it is very difficult to effectively refine the grain size of Al–Si based foundry alloys due to the poisoning effect of Si on the potent nucleation particles. By forming Ti–Si based intermetallic phases on the surface of TiB_2 particles [15–18], the potency of the particles in nucleating α-Al grains is significantly reduced. Addition of Ti alone has also the influence of grain refinement, however, the minimum addition amount of Ti needs to be more than 0.2wt% [19,20]. When B element is added at the same time, the minimum Ti content added is related to the amount of B. When enough B element is added, the minimum Ti content needed is 0.02 wt.%, by which a good grain refinement effect can be achieved [21,22]. The AlSiTi phase can be avoided when the Ti content is less than 0.1–0.11 wt.% [23].

Sc, as a rare earth element, has been found to have the influence of both refining α-Al grains and modifying Al–Si eutectics in Al–Si based foundry alloys [6,24–33]. However, to reach a sufficient grain refinement effect, the addition level of Sc has to be higher than certain minimum level dependent of Si contents in the alloys, for example 0.5wt.% in A356 alloy [34]. In binary Al–Sc alloys and Al–Mg-Sc alloy, it is found that the grain refining effect of Sc on aluminum alloy is mainly due to the interaction between Sc and Al forming Al_3Sc particle during solidification, which can act as potent nucleation sites for Al grains [35,36]. Al_3Sc has a cubic $L1_2$ crystal structure [35,37], and its lattice constant is very close to that of α-Al, and the lattice disregistry between Al_3Sc and α-Al mismatch is less than 1.25% [38]. Based on the mechanism, Xu et al. [28,39] suggested $L1_2$ structured Al_3Sc is also responsible for the grain refinement in Al–Si–Mg foundry alloys. However, such a mechanism may not be applicable to explain the grain refinement effect in Al–Si based foundry alloys. According to the calculated phase diagrams for Al–Si–Mg-Sc system by Lu et al. [6,27], $AlSi_2Sc_2$ phase, instead of Al_3Sc particles, is the first intermetallic phase to precipitate in liquid Al when the Sc content is higher than ternary eutectic points. The authors therefore suggested that the grain refinement by Sc addition is due to the increased grain growth restriction factor during solidification.

The modification mechanism of Sc on eutectic Si is still under debate. Based on the twins observed in eutectic Si modified by Sc , Xu et al. [7,28] proposed that the modification of eutectic Si by Sc conforms to the IIT mechanism. They have also shown that the addition of Sc decreases the growth temperature of Al–Si eutectics. Lu et al. [6,27] attributed the refinement of eutectic Si particles by Sc addition to the formation of finer ternary eutectic (Al) + Si + $AlSi_2Sc_2$ instead of binary eutectic (Al) + Si structure. It was also found that $AlSi_2Sc_2$ particles are coherent with primary/eutectic Al phase. To reach a sufficient modification effect, the addition level of Sc was suggested to be higher than the ternary eutectic point dependent of Si contents in the alloys, for example 0.54wt.% in A356 alloy [6]. However, the work by Prukkanon et al. [30] showed that an addition of 0.2 wt.% Sc can lead to a significant modification effect on eutectic Si particles in Al6Si0.25 Mg alloy, where the Sc addition level is much lower than the ternary eutectic point.

It is well known that the grain refinement effect and modification of Al–Si eutectics are largely affected by the cooling rate during casting. However, how Sc addition influences the microstructure and properties of Al–Si–Mg foundry alloys under different cooling rate conditions has not been well studied. This work is aimed at a further clarification of the mechanisms for the grain refinement and modification of eutectic Si in Al–Si–Mg alloy by Sc addition. The effects of cooling rates on the grain refinement and eutectic modification will also be addressed by using wedge-shaped casting samples.

2. Experimental procedures

The experimental alloys were prepared from 99.9wt% commercially pure aluminum, pure silicon, commercially pure magnesium, Ti powder and Al-5Sc master alloy. The alloy was melted in a resistance furnace. The chemical compositions of the alloys were determined by emission spectrometry and were listed in Table 1.

To study the effect of the cooling rate on the microstructure and the mechanical properties, the melt was poured at 700 °C into the wedge-shaped metal mold preheated to 300 °C. Before pouring, argon was used for degassing of the melt for 20 min. The shape and size of the casting were shown in Fig. 1 (a).

The positions to cut tensile specimens in the casting are shown in Fig. 1 (b). The shape and dimensions of the tensile specimen are shown in Fig. 1 (c).

8 tensile specimens were taken from each wedge casting of the Sc-free alloy and Sc-added alloy (from bottom to top) by wire cut electrical discharge machining, and the tensile test was carried out on Instron 3382 electronic tensile machine. The fractures morphology of tensile specimens was observed by scanning electron microscope (SEM) using an FE-SEM SU5000 (Hitachi High-Tech Corp.) equipped with energy dispersive X-ray spectroscope (EDSX; TSL, Digiview). The transmission electron microscopy (TEM) samples were prepared by ion-beam thinning using Gatan 691 and were observed using FEI Tecnai G2 F20 operated at 200 kV.

In order to record the local cooling rate at different locations of the wedge castings during solidification, 4 thermocouples of K-type were placed at 2#, 4#, 6#, 8# tensile specimen locations in the mold before casting. The cooling curves were collected by using GRAPHTEC GL840.

Table 1 – Chemical Compositions of alloys.

Alloy	Element (weight percent)					
	Si	Mg	Sc	Fe	Ti	Al
Al–Si–Mg–Ti	6.8	0.59	0	0.08	0.24	Balance
Al–Si–Mg–Ti-Sc	6.9	0.58	0.52	0.07	0.25	Balance

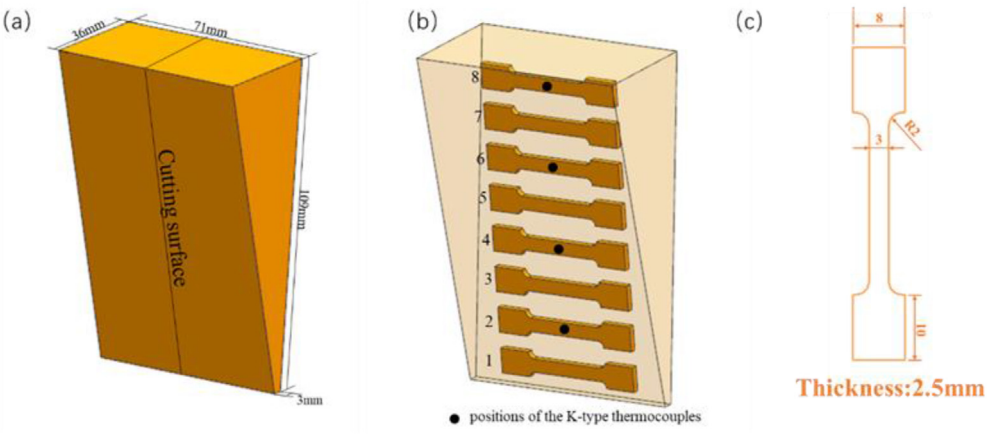

Fig. 1 – Schematic drawings of the casting block obtained by wedge casting: (a) Shape and dimensions of casting block; (b) Positions of tensile specimens and K-type thermocouples in casting block; (c) Shape and dimensions of the tensile specimen.

In order to analyze the solidification grain structure in the casting block, mechanically polished samples were anodized by using a DC power of 30V and 0.35A current and a corrosion solution containing sulfuric acid, phosphoric acid and water with a volume ratio of 38:43:19. The anodized samples were observed under the polarizing mode of Zeiss Scope-A1 metallographic microscope. The grain size was determined by using the linear intercept method. To reveal the 3D morphology of eutectic Si phase, a deep etching of well-polished sample surface by 20% NaOH aqueous solution for 60 min was applied.

To understand the influence of Sc on the solidification process of the experimental alloys, Thermo-Calc was applied to calculate corresponding phase diagrams of the alloys, by using the thermodynamic database TCAl 8.

3. Results

3.1. *Influence of Sc addition on the solidification cooling curve*

Fig. 2 shows the local cooling curves of 2#, 4#, 6#, and 8# tensile specimens in Sc-free alloy and Sc-added alloy. As can be seen, with the decrease of the cross section of casting the initial cooling rates increases. The measured initial cooling rate before precipitation of primary α-Al grains are 21.4, 19.4, 13.6, 11.1K/s, respectively, while the average solidification cooling rates from primary phase to eutectic reaction are 6.8, 3.5, 2.2, 1.8K/s, respectively, in Sc-free alloy. In Sc-added alloy, the initial cooling rates are 24.5, 20.5, 13.9, 7.6K/s, and the cooling rates from primary phase to eutectic are 6.9, 6.5, 5.5, 2.4 K/s respectively.

From the cooling curves, two solidification reactions, formation of primary α-Al grains in the liquid metal and eutectic reaction, can be clearly identified. As can be seen from Fig. 2(a), for the Sc-free alloy, recalescence plateau can be clearly observed in 6# and 8# sample at about 610.9 and 612.2 °C (corresponding to the lowest cooling rates in the first derivative curves), indicating the massive precipitation of α-Al grains. However, in 2# and 4# samples, no recalescence plateau is presented, which should be attributed to the much higher cooling rates. For the Sc-added alloy, none of the cooling curves show clear recalescence plateau for the formation of α-Al grains. As labeled in the figures, at the same locations in the castings (corresponding to similar initial cooling rate), the Sc-added alloy always has higher

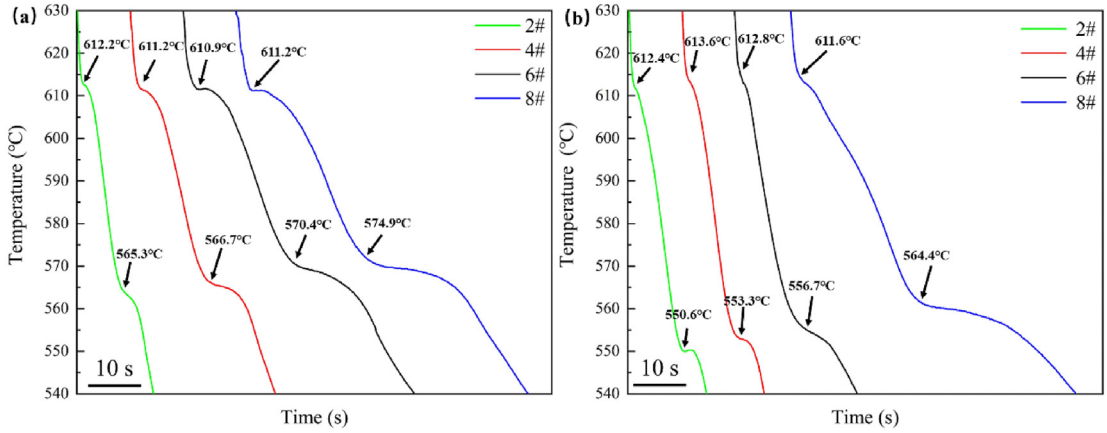

Fig. 2 – Local cooling curves of alloys during solidification: (a) Sc-free alloy; (b) Sc-added alloy.

temperatures for massive precipitation of α-Al grains than the Sc-free alloy, indicating that Sc addition has enhanced the heterogeneous nucleation of α-Al grains to higher temperatures.

The temperatures of maximum transformation rate of eutectic reaction (corresponding to the lowest cooling rate in first derivative curves) are also labeled in each cooling curves in Fig. 2. It can be clearly seen that the addition of Sc significantly reduces the eutectic growth temperature. It implies the addition of Sc has the influence of suppressing the nucleation of Al–Si eutectics in the alloy. Another observation is that the eutectic solidification temperature decreases with increasing cooling rate, which is the same for both alloys.

3.2. *Refinement of α-Al grains by Sc addition*

Fig. 3 shows the grain structure of Sc-free alloy. All the samples have coarse equiaxed grains with well-developed equiaxed dendrite arms, with grain sizes larger than 240 μm. The equiaxed grain structure implies that the addition of Ti has played a role in refining the grain structure, although the grain refinement effect is rather weak. It can also be seen that with

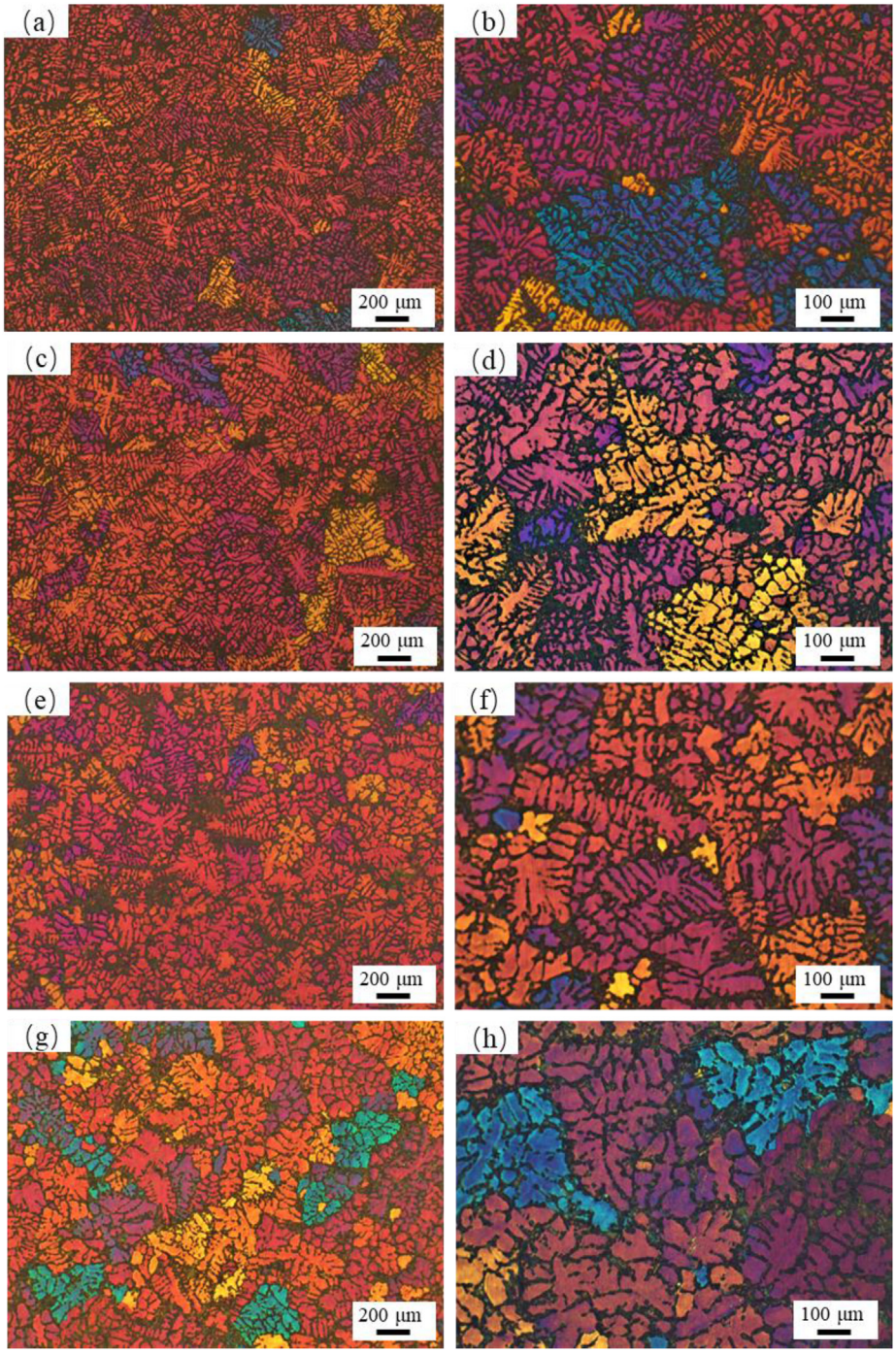

Fig. 3 – Grain morphology at different tensile specimen areas in Sc-free alloy: (a) (b) 2#; (c) (d) 4#; (e) (f) 6#; (g) (h) 8#.

decrease of cooling rate, grain size becomes larger and the dendrite arms become coarser.

Fig. 4 shows the grain structure of Sc-added alloy under polarized light. In comparison to the grain structure of Sc-free alloys, the solidification grains are significantly refined by Sc addition. For the samples with lower cooling rates, 6# and 8#, a large fraction of the grains shows a globular morphology, where dendrite arms are difficult to distinguish. It means a significant ripening of dendrite arms has happened during solidification.

Fig. 5 summarizes the measured grain size and Dendrite Arm Spacing (DAS) of Sc-free alloy and Sc-added alloy. It can be seen from Fig. 5 (a) that the average grain size of both Sc-free and Sc-added alloy decreases with increasing cooling rate. The average grain sizes of 8# and 1# samples of Sc-free alloy are 307.7 μm and 241.6 μm, respectively. In Sc-added alloy, the average grain sizes of 8# and 1# samples are 177.9 and 115.7 μm, respectively. An impressive grain refinement has been achieved by addition of Sc. Fig. 5(b) shows the measured DAS of Sc-free alloy and Sc-added alloy. It can be

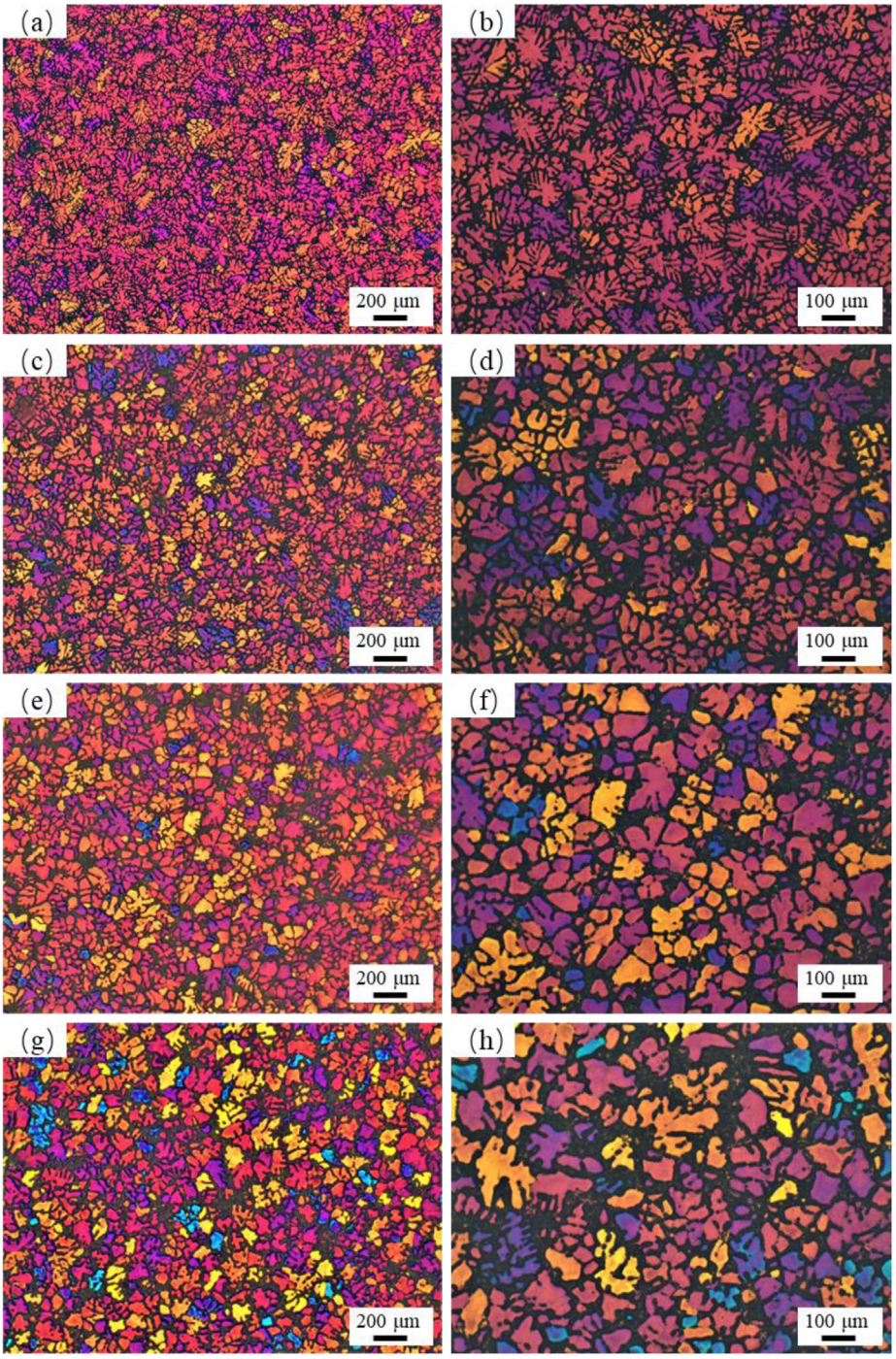

Fig. 4 – Grain morphology at different tensile specimen areas in Sc-added alloy: (a) (b) 2#; (c) (d) 4#; (e) (f) 6#; (g) (h) 8#.

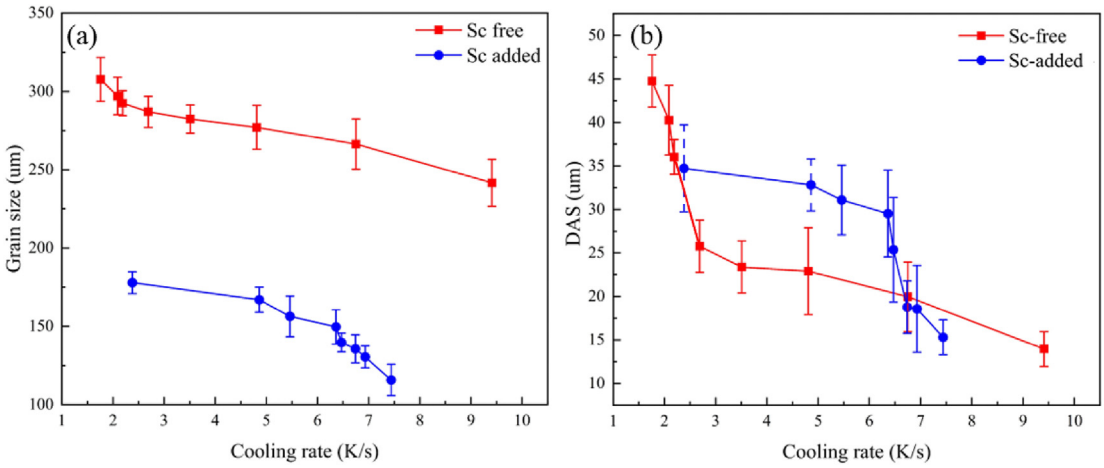

Fig. 5 – Grain size and Dendrite Arm Spacing of Sc-free alloy and Sc-added alloy.

seen that with increasing of cooling rate, the DAS of Sc-free alloy decreases from 44.8 μm (8# sample) to 14.0 μm (1# sample), and the DAS of Sc-added alloy decreases from 34.7 μm (6# sample) to 15.3 μm (1# sample).

Fig. 6 shows a typical BSE-SEM image for the solidification structure of Sc-added alloy sample and corresponding EDX elemental mapping. In addition to fine Al–Si eutectics, some eutectic Mg_2Si and script-like $AlSc_2Si_2$ particles can also be occasionally observed in the interdendritic region. To reveal the effect of Sc addition on the grain refinement, the heterogeneous nucleation sites of α-Al grains have been carefully searched by using backscattered electron (BSE) SEM images. Plate shaped particles with a light grey contrast can be frequently observed in the center of equiaxed α-Al grains (pointed by a yellow arrow), which are supposed to have acted as the heterogeneous nucleation sites for Al grains. EDX elemental mapping analyses show that the particles contain a high fraction of Ti content, in addition to Sc and Si, implying that a new phase, different from $AlSc_2Si_2$, has formed and acted as the nucleation sites for Al grains.

To further study the crystal structure of the (Ti, Sc)-rich particles and their orientation relationship to the surrounding Al grain, Lift-Out technique was used to cut a thin TEM sample containing both the particle and Al matrix. Fig. 7(a) shows a low magnification TEM image of the sample. The TEM-EDS spectra and the measured chemical composition of the particle measured are shown in Fig. 7 (b1, b2). The unmarked peak in energy spectrum is caused by copper bracket. As shown, this particle is enriched with Ti, Sc, and Si, which confirms the SEM-EDX analyses. the measured chemical compositions of the particle show that they have about two times (Ti + Sc) atomic content as Si content, which is different from the eutectic $AlSc_2Si_2$ phase. Instead, the composition of the particle is very close to $(Al, Si)_3(Ti, Sc)$. The selected area electron diffraction (SAED) patterns of $(Al, Si)_3(Ti, Sc)$ taken along the [010] zone axis and the $[\bar{1}\,10]$ zone axis are shown in Fig. 7 (b3) and (b4), respectively. It is determined that particle has a tetragonal crystal structure with a = 0.38 nm and c = 0.86 nm, suggesting that the $(Al, Si)_3(Ti, Sc)$ phase has the same crystal structure as $D0_{22}$-Al_3Ti (a = 0.3846 nm and c = 0.8594 nm) and similar lattice constants.

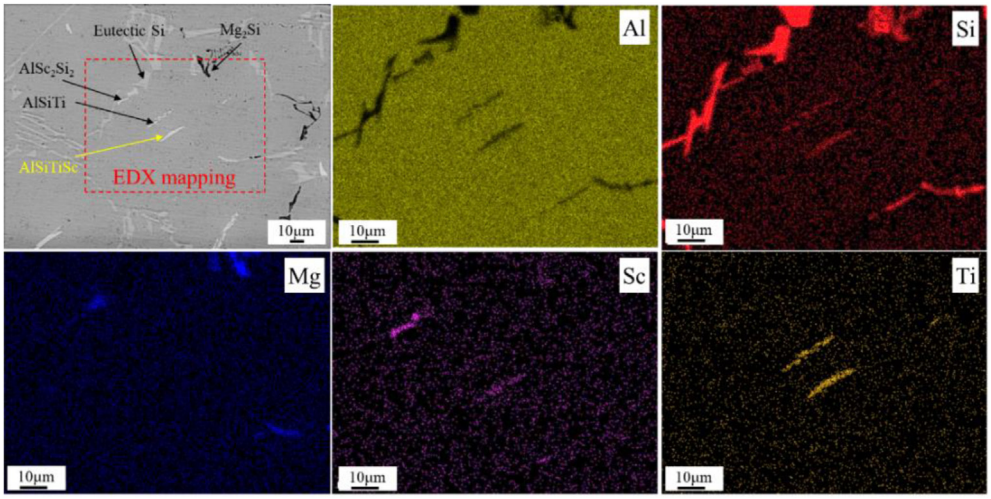

Fig. 6 – Backscattered electron (BSE) SEM micrograph and EDX spectrum of heterogeneous nucleus in Sc-added alloy.

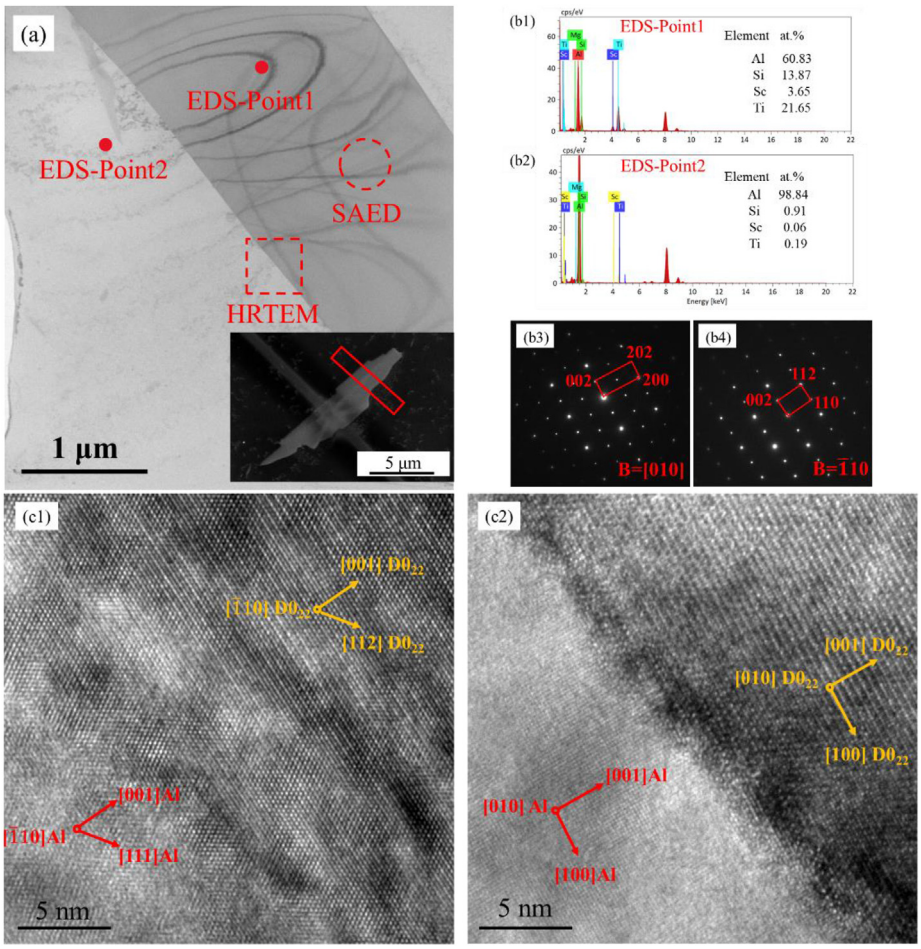

Fig. 7 – TEM images of heterogeneous nucleus in Sc-added alloy: (a) Bright-field image of heterogeneous nucleus (b1) (b2) EDS analysis (b3) SAED image along [001] (b4) SAED image along [$\bar{1}$10]; (c) The interface between α-Al and (Al, Si)$_3$(Ti, Sc) (c1) (c2) HRTEM images.

Fig. 7 (c1) and (c2) show the HRTEM images of D0$_{22}$-(Al, Si)$_3$(Ti, Sc) and α-Al taken along <110>Al and <100> Al zone axes, respectively. Several parallel atomic plane pairs between the (Al, Si)$_3$(Ti, Sc) phase and α-Al matrix can be found and the two phases show a strong orientation relationship (OR). The OR can be written as:

[$\bar{1}$10] D0$_{22}$//[$\bar{1}$10] Al (112)D0$_{22}$//(111) Al

This OR is in good agreement with the OR between Al_3Ti phase and Al phase [40]. It is well known that Al_3Ti is a potent heterogeneous nucleation sites for α-Al grains during solidification. Here the D0$_{22}$-(Al, Si)$_3$(Ti, Sc) particles are suggested to have played the same role as Al_3Ti.

3.3. *Modification of eutectic Si by Sc*

Fig. 8 shows the morphology of eutectic Si in the as-cast samples after deep etching. In the Sc-free alloy, the eutectic Si particles show a typical plate-shaped morphology. The size of eutectic Si in the 2# specimen (Fig. 8(a)) is significantly smaller than that of 8# specimen (Fig. 8 (b)), showing the strong influence of cooling rate on the size of eutectic Si particles.

As can be seen from Fig. 8 (c) and Fig. 8 (d), the morphology of eutectic Si in Sc-added alloy has changed from the plate-shaped into fibrous morphology, showing a similar modification effect as Sr addition. This is in agreement with the observations by Xu et al. [24,28]. By comparing 2# specimen (Fig. 8 (c), local cooling rate 6.9 K/s) with 8# specimen (Fig. 8 (d), local cooling rate 2.4 K/s), one can also see the influence of solidification cooling rate on the modification effect: the higher the cooling rates the finer the eutectic Si fibers.

3.4. *Mechanical properties*

Fig. 9 (a) shows the tensile strain-tensile stress curves of casting samples of different cooling rates for both Sc-free and Sc-added alloys, with the measured yield strength presented in Table 2. The measured ultimate tensile strength (UTS) and elongation of different specimens as a function of cooling rate has been summarized in Fig. 9(b) and (c), respectively. As a general trend, UTS, yield strength and elongation of the Sc-free alloy increase with increasing solidification cooling rate, and the Sc-added alloy shows higher UTS and yield strength than Sc-free alloy at all the experimental solidification cooling rate conditions. More interestingly, the UTS, yield strength and elongation of Sc-added alloy show much less sensitivity to solidification cooling rate than the Sc-free alloy. More

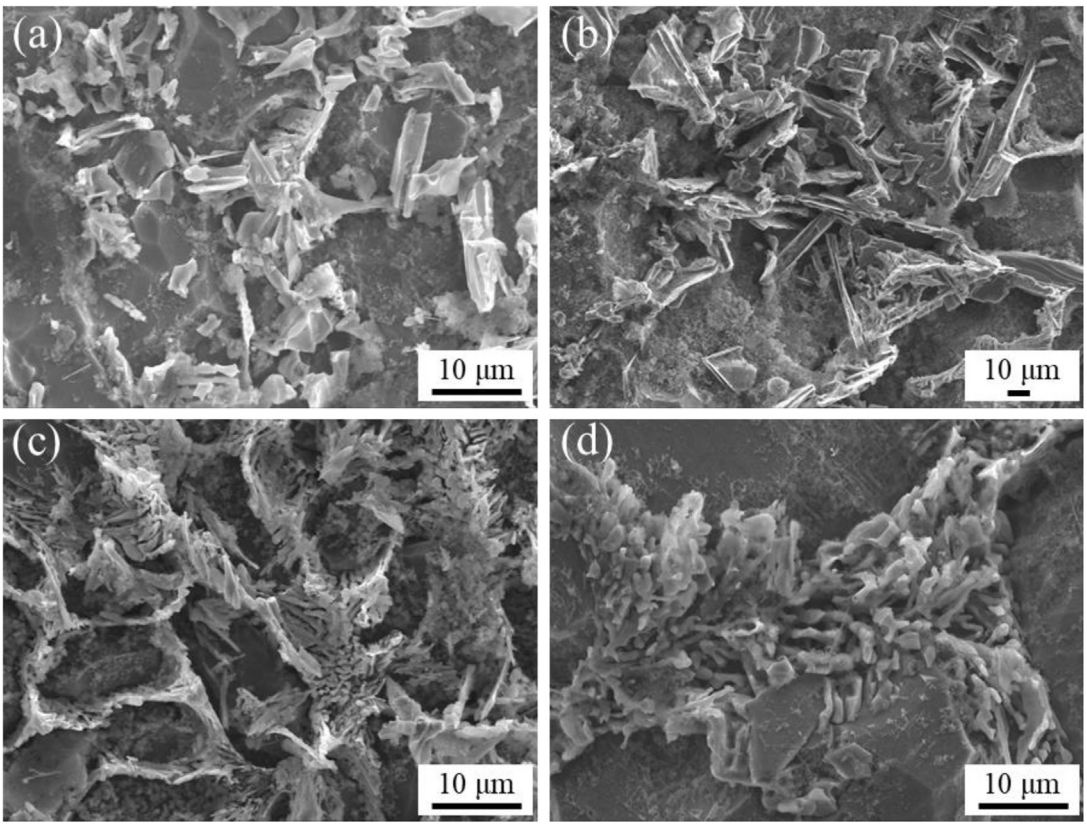

Fig. 8 – Morphology of eutectic Si in Sc-free alloy and Sc-added alloy: (a) 2# specimen (6.8 K/s) of Sc-free alloy; (b) 8# specimen (1.8 K/s) of Sc-free alloy; (c) 2# specimen (6.9 K/s) of Sc-added alloy; (d) 8# specimen (2.4 K/s) of Sc-added alloy.

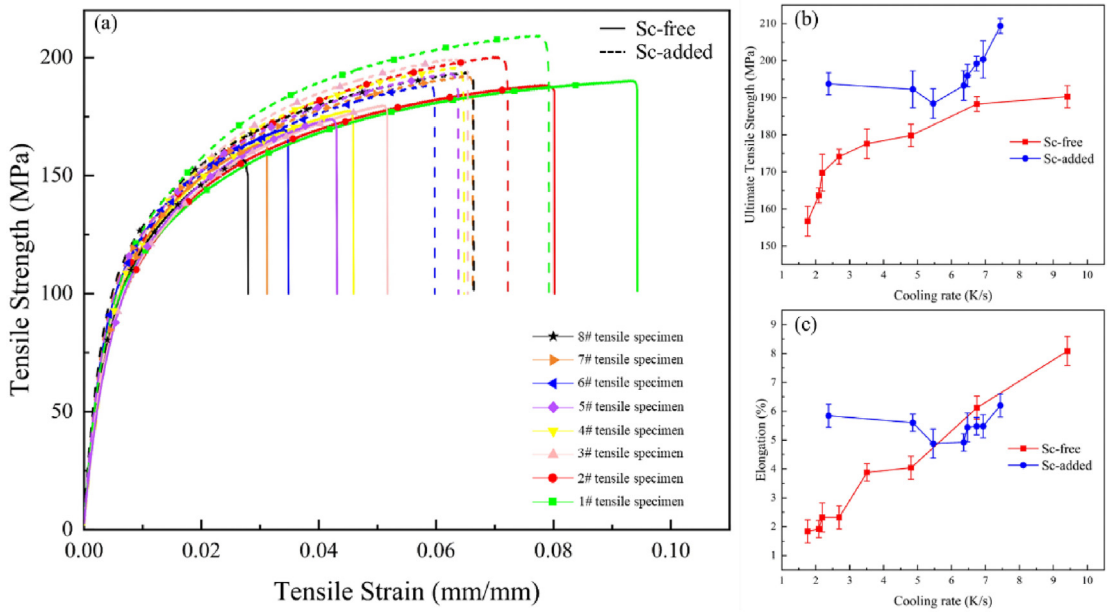

Fig. 9 – Mechanical properties and elongation of Sc-free alloy and Sc-added alloy: (a) Engineering stress–strain curves of Sc-free alloy and Sc-added alloy; (b) Ultimate tensile strength; (c) Elongation.

Table 2 – Yield strength of Sc-free alloy and Sc-added alloy.

Samples	alloy	1#	2#	3#	4#	5#	6#	7#	8#
Yield strength (MPa)	Sc-free	127.1	126.2	116.0	115.5	115.0	114.3	109.7	106.2
	Sc-added	137.8	130.5	129.5	129.1	128.9	125.8	130.3	132.8

specifically, when the local cooling rate is less than 2K/s (Specimen 7 and 8), the Sc-free alloy shows substantially lower strength (UTS <163 MPa) and elongation (<2.5%) than those of high cooling rates (e.g., specimen 1). In contrast, although the Sc-added alloys show an increase of UTS and elongation at higher cooling rates, high elongation (~5%) and high UTS (>185 MPa) can also be achieved in 7# and 8# specimens.

Fig. 10 shows TEM images of the 8# tensile specimen of Sc-added alloy. Surprisingly, a high density of nano-sized globular precipitates with diameter of about 10 nm can be observed in the α-Al matrix. These small particles are identified as $L1_2$ structured Al_3Sc particles by HRTEM image (Fig. 10 b) and fast Fourier transformation (FFT) analysis (Fig. 10 c). The volume fraction of the Al_3Sc precipitates is about 0.44%. The general increase of yield strength and UTS of the Al–Si–Mg alloy at different cooling rate conditions by Sc-addition should be partially attributed to the dispersion strengthening effect by Al_3Sc precipitates. It has been suggested by many researchers that Al_3Sc particles could act as heterogeneous nucleation sites for Al grains during solidification. However, such nano-sized Al_3Sc particles are too small to act nucleation sites for α-Al grains, as the free growth undercooling for grain nucleation on these grains will be too high to achieve during normal casting process. Instead, these Al_3Sc particles should have precipitated from Al matrix during cooling process. Since the metal mold was pre-heated to 300 °C before casting, the wedge samples could stay for a relatively long time at temperatures higher than 350 °C [41], which was determined by experimental cooling curves to be about 585 s. With the decrease of cooling rate, the time that samples stayed at temperature higher than 350 °C gradually increase. In other word, the decrease of cooling rate led that samples have longer time to form more Al_3Sc precipitates. However, the decrease in cooling rate did not result in a significant increase in grain size that is 20 μm and DAS (4 μm). These are why the UTS and elongation decrease with the increasing cooling rate for Sc-added alloy when cooling rate is lower than 6 K/s.

Fig. 10(d) shows a bright-field TEM image including some Al_3Sc precipitates and dislocations. It can be seen that the dislocations showed in Fig. 10(d) bypass rather than cross the Al_3Sc precipitates. Therefore, the strengthening mechanism of Al_3Sc belong to Orowan strengthening. The inability to be sheared of Al_3Sc and the strongly coherent between Al_3Sc and α-Al determine the excellent properties of Sc-added alloy [42].

Fig. 11 shows two representative SEM images of fracture morphology of 8# tensile specimens of both alloys. As can see, both specimens show quasi-cleavage fracture topograph. The cleavage facets are due to the brittle crack propagating along Al–Si eutectic structures. As a comparison, the cleavage facets of Sc-added alloy are much smaller than those of Sc-free sample, due to the refined eutectic Si crystals. Also, there are more and deeper dimples in the Sc-added alloy, showing that Sc addition has improved the ductility of the alloy.

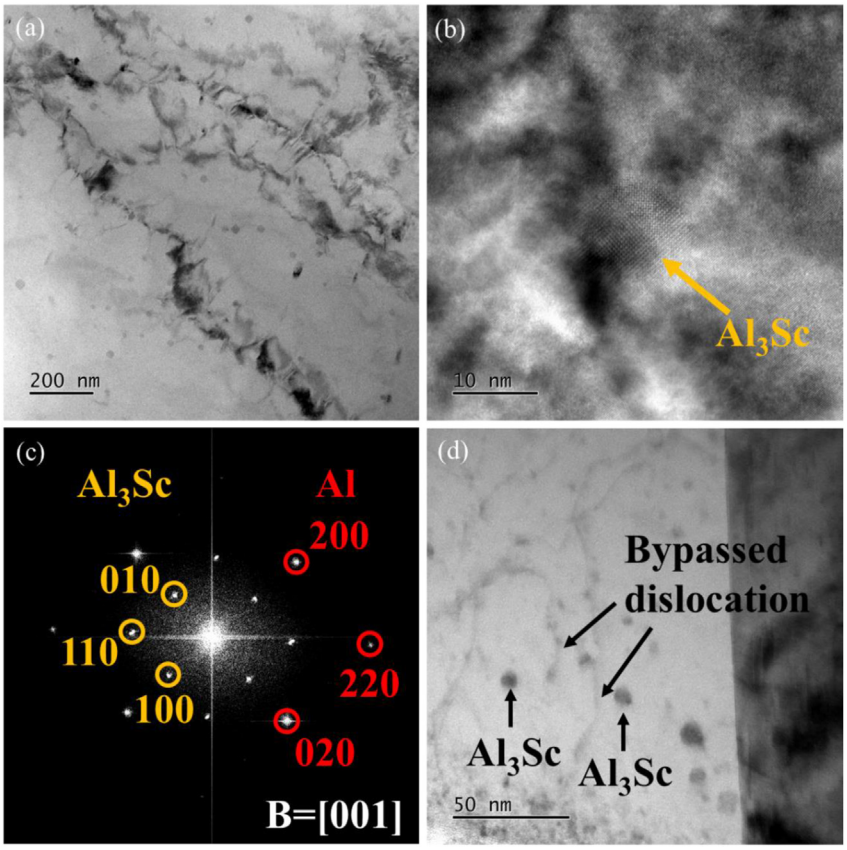

Fig. 10 – TEM observation of Al_3Sc particles: (a) TEM image of Al_3Sc particles; (b) high-resolution image of Al_3Sc; (c) diffraction spot images; (d) interaction between Al_3Sc and dislocation.

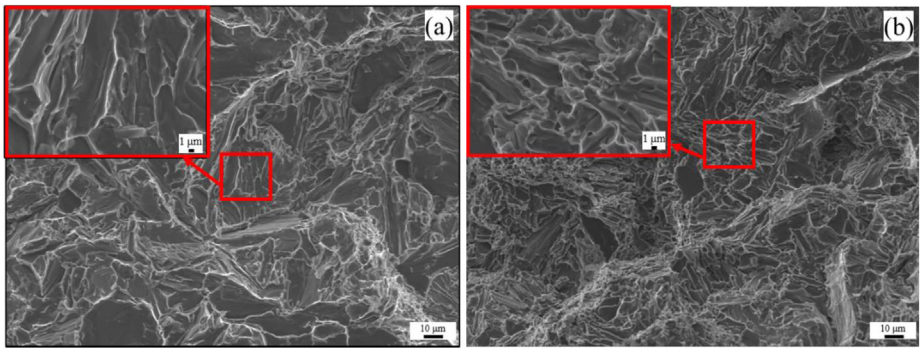

Fig. 11 – Fractographs of the tensile specimen from as-cast: (a) 1# tensile specimen of Sc-free alloy; (b) 8# tensile specimen of Sc-free alloy.

4. Discussion

4.1. *Grain refinement*

The experimental results in the present work confirm the strong grain refinement effect of Sc addition in Al–Si–Mg based foundry alloys. As a general trend, the grain refinement effect increases with increasing cooling rate. It has to be mentioned that the as-cast Sc-free reference alloy also shows an equiaxed grain structure, though coarse. This should be attributed to the high Ti content in the alloy, over the peritectic content, 0.15 wt.%. As a result, the peritectic Al_3Ti particles could form during solidification and act as nucleation sites for Al grains. The coarse grain structure should be due to the relatively low grain refinement potentials of Al_3Ti particles. It has been shown by Liu et al. that even with an addition of 1.5 wt.% Ti, as-cast A356 alloys still show a rather coarse equiaxed grain structure [43].

It has been a topic of debate on the grain refinement mechanism by Sc addition in Al–Si based foundry alloys. In Al–Sc binary alloys, it was shown that the Sc content has to be higher than the eutectic point, 0.55 wt.%, in order to form $L1_2$ structured primary Al_3Sc particles during solidification and thus achieve significant grain refinement effect [35,36,44]. It was also shown that an addition of Ti to Al–Sc alloy can improve the nucleation efficiency by forming Al_3(Sc, Ti) particles [44]. Both Al_3Sc and Al_3(Sc, Ti) primary particles show cube shapes at low solidification cooling rates. In the present Sc-added Al–Si–Mg–Ti alloy, the plate shaped Sc-containing particles frequently observed in the center of Al grains are determined to have a constitution close to (Al, Si)$_3$(Sc, Ti) particles, which are suggested to have formed as the heterogeneous nucleation sites for Al grains. Their morphologies are obviously different from those reported Al_3(Sc, Ti) or Al_3Sc particle forming through the over eutectic reaction. It implies that the formation of (Al, Si)$_3$(Sc, Ti) particles is not due to the same over eutectic reaction. In Al–Si based foundry alloys, due to the high content of Si, the solidification path of Sc-added A356 alloy is largely different from the Al–Sc or Al-Sc-Ti alloys. Based on the Al–Si–Mg-xSc phase diagrams calculated by using CALPHAD method, Lu et al. [6,27] suggested that $AlSc_2Si_2$ particles will form as a eutectic phase through a ternary eutectic reaction or as a primary phase when the Sc content is larger than the ternary eutectic point. However, this ternary eutectic temperature is quite low, at about 570 °C. Even at 1.0wt % Sc content, the formation temperature of primary $AlSc_2Si_2$ is about 604 °C, which is much lower than the detected nucleation temperature of Al grains in the present alloy, 611–614 °C. It implies that $AlSc_2Si_2$ can not act as the nucleation site of Al grains, although it was shown to have a coherent interface with Al phase [27]. The different solidification and grain refinement behavior in the present Sc-added alloy than the previous Sc added A356 alloys may be due to the Ti content.

To understand the solidification path of the present alloy, a phase diagram of Al-6.9Si-0.6Mg-0.25Ti-xSc has been calculated by Thermo-Calc, using TCAl8 data base. As can be seen from Fig. 12, for the Sc-added experimental alloy, the primary phase forming during solidification is Al_3Ti phase at temperatures above the formation temperature of Al grains. At 595 °C, $AlSi_3Ti_2$ could form in the liquid, after which $AlSc_2Si_2$ phase will form as a product of hypereutectic reaction. Since $AlSc_2Si_2$ phase form at much lower temperatures than primary Al phase, $AlSc_2Si_2$ particles should distribute within interdendritic regions of Al grains. The result is in agreement with experiment result shown in Fig. 12. Instead, the heterogeneous nucleation sites should be peritectic Al_3Ti based phase, where part of Ti atoms are replaced by Sc atoms while part of Al atoms are substituted by Si atoms. According to the results of first-principles calculation [45–47], Si atoms tend to substitute Al sites in Al_3Sc forming (Al, Si)$_3$Sc due to the atomic radius of Si atom is similar to that of Al atom. Similar phenomenon may also occur in Al_3Ti. Unfortunately, such (Al, Si)$_3$(Ti, Sc) phase is not included in the thermodynamic database. From the phase diagram, we can also see that $AlSi_3Ti_2$ always form at temperatures lower than Al phase, which explains why the poisoning effect by Si on grain refinement effect could be avoided in the present Al–Si–Mg–Ti alloys and Sc-added alloy.

4.2. *Modification*

In unmodified commercial Al–Si foundry alloys, the eutectic Si phase tends to form as coarse flake-shaped particles during solidification. This can be attributed to the unavoidable impurity alloying element P in cast aluminium alloys. It has been shown, even with a concentration of several ppm, P can interact with Al forming AlP particles [48], which act as nucleation sites for Si particles. As a consequence, Si phase

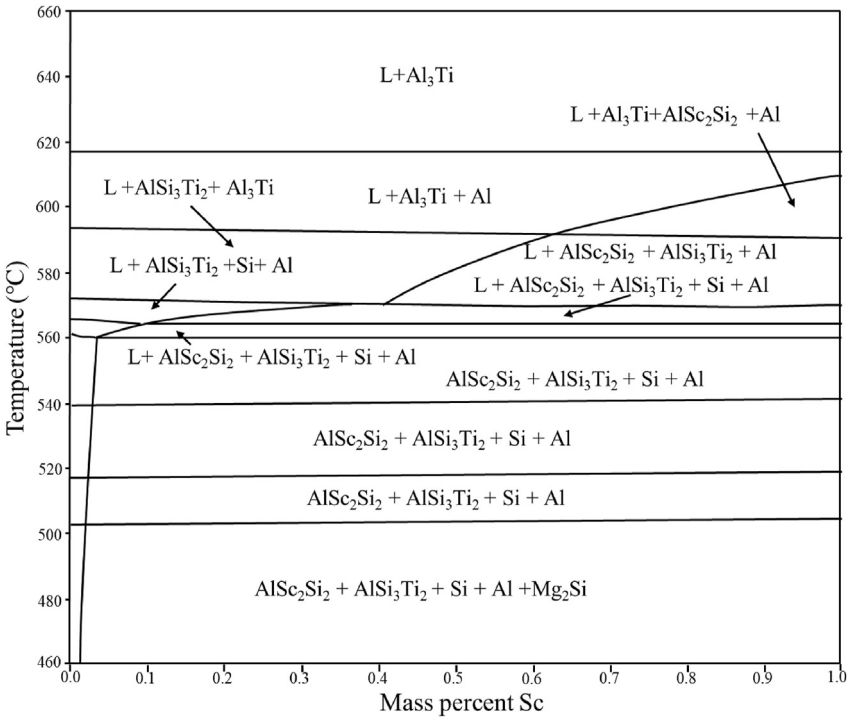

Fig. 12 – The phase diagram of Al-6.9Si-0.6Mg-0.25Ti-xSc calculated by Thermo-Calc.

will be the leading phase of Al–Si eutectic growth. With a fast faceted growth kinetics, the eutectic Si will grow into coarse plates. This is exactly the case of the Sc-free alloy in the present work. In the Sc-added alloy, the thermal analyses show clearly that the Sc addition significantly reduces the eutectic growth temperature. It can be safely suggested that Sc can also react with P in the liquid, suppressing the formation of AlP particles [49]. It has been found that Ca-addition has the same effect in reducing the Al–Si eutectic growth temperature [50], However, different from Ca-addition which has only the effect of refining the eutectic plates, Sc addition also changes the eutectic Si into fibrous structure. It implies that Sc may have the effect of enhancing the twinning of Si crystals, similar to Sr modification. To verify this hypothesis, some high-resolution TEM study on the eutectic Si particles is necessary in the future work. It is worth of mentioning, the modification effect by Sc addition in this work is different from that reported in Al-xSi-xSc alloy by Lu et al. [6,27], where the refinement of eutectic Si phase is attributed to the ternary eutectic reaction. In this work, only limited amount of $AlSc_2Si_2$ phase could be detected.

4.3. *Mechanical properties*

Fig. 13 clearly shows that Sc-addition significantly improves both the yield strength and UTS of Al–Si–Mg–Ti alloy in the as-cast state. The yield strength increase can be attributed to the precipitation of nano-sized Al_3Sc particles, which provide a dispersion hardening effect. Since Al_3Sc precipitates could precipitate in the as-cast state, it means that a relatively high super-saturation of Sc in solid solution could be achieved in the alloy during solidification. This is important for the castings which are supposed to be used in the as-cast state.

The almost linear increase of elongation of Sc-free alloy with cooling rate could be attributed to the decrease of dendrite arm spacing (DAS) of Al grains with increasing solidification cooling rate. It is well known that the size and morphology of Al–Si eutectics have a strong influence on the ductility of Al–Si base foundry alloys. At higher solidification cooling rate, finer eutectic Si plates and smaller lamellar spacing can be achieved. At the same time, the size of eutectic cells also decreases with decreasing with DAS due to the constrain of Al dendrite arms. In contrast, the elongation of Sc-added alloy does not show the monotonic decrease with decreasing initial solidification cooling rate. Although due to the strong ripening of dendrite arms at low solidification

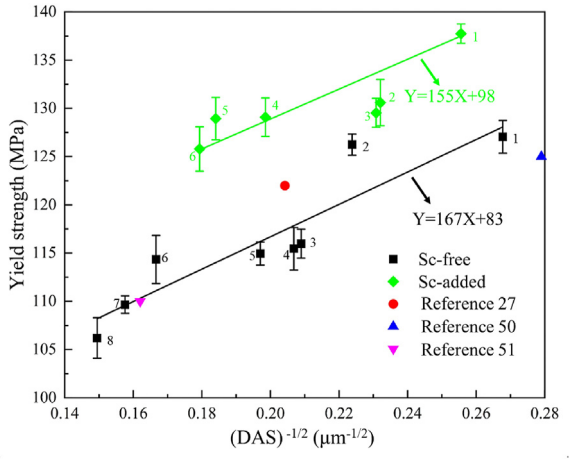

Fig. 13 – Yield strength vs. inverse square root of DAS obtained from the tensile test of Sc-free alloy and Sc-added alloy.

cooling rates the grains of 7# and 8# samples show relatively large DAS, the two samples have a relatively high elongation ~4.9%. This should be attributed to the modification effect of Sc on the eutectic Si particles.

According to Hall–Petch equation, the yield strength (σ) of alloys has a linear relationship to the inverse square root of the grain size d, which has been well validated by many different metallic materials. However, for Al–Si based foundry alloys the strength is more dependent of DAS than grain size because there is a large fraction of eutectic Si particles and intermetallic particles distributing in the interdendritic regions. This has been proved by several experimental studies [27,51,52] which showed that the yield strength of hypoeutectic Al–Si alloys is more relevant with DAS than grain size according to Hall–Petch equation. So, we have used the DAS instead of grain size for the d value in the following equation, where σ_0 is yield strength of single crystal and k a constant:

$$\sigma = \sigma_0 + \frac{k}{\sqrt[2]{d}}$$

Fig. 13 shows the relationship between DAS and yield strength of Sc-free alloy and Sc-added alloy. As can be seen, both alloys show linear relationship between the yield strength and square root of DAS. However, the fitted σ_0 value of Sc-added alloy (98 MPa) is obviously higher than that of Sc-free alloy (83 MPa), which confirms the dispersion hardening effect of nano-sized Al_3Sc in the Sc-added alloy.

5. Conclusions

The effects of Sc on the as-cast microstructures and mechanical properties of Al–7Si-0.6Mg-0.25Ti alloy at different cooling rates have been studied based on the wedge-shaped casting test. The following conclusions can be drawn.

(1) A significant grain refinement effect has been achieved in Al–7Si-0.6Mg-0.25Ti alloy by Sc addition. It is found that the plate-shaped $(Al, Si)_3(Ti, Sc)$ particles that formed as a peritectic reaction product have acted as heterogeneous nucleation sites for α-Al grains during solidification.
(2) The addition of Sc has a strong modification effect on Al–Si eutectics, changing the eutectic Si from plate shape into fibrous morphology. The reason can be attributed to the significantly reduced Al–Si eutectic growth temperature by Sc addition.
(3) The addition of Sc has shown strong effects in improving the strength and elongation of the alloy at all the experimental solidification cooling rate conditions. More importantly, Sc addition has significantly reduced the strong sensitivity of the strength and ductility Al–Si–Mg foundry alloys to solidification cooling rate. Especially at all the experimental cooling rates, the elongation of Sc-added Al–Si–Mg alloy is higher than 4.9%.
(4) Precipitation of high-density nano-sized Al_3Sc precipitates has been observed in the Sc-added alloy in the as-cast state, which contributes to the strength improvement of the alloy.

Data availability

Data will be made available on request.

Declaration of competing interest

The authors declare that they have no known competing financial interests or personal relationships that could have appeared to influence the work reported in this paper.

Acknowledgement

This research work was financially funded by the Natural Science Foundation of Shanxi Province (202103021224179); Shanxi Province Postgraduate Education Innovation Project (2022Y613); Shandong Province Science and Technology Innovation Capability Enhancement Project (2022TSGC2201).

REFERENCES

[1] Li D, Cui C, Wang X, Wang Q, Chen C, Liu S. Microstructure evolution and enhanced mechanical properties of eutectic Al–Si die cast alloy by combined alloying Mg and La. Mater Des 2016;90:820–8.
[2] Bolzoni L, Nowak M, Hari Babu N. Grain refinement of Al–Si alloys by Nb–B inoculation. Part II: application to commercial alloys. Mater Des 2015;66:376–83.
[3] Hekmat-Ardakan A, Ajersch F. Thermodynamic evaluation of hypereutectic Al–Si (A390) alloy with addition of Mg. Acta Mater 2010;58(9):3422–8.
[4] Cáceres CH, Davidson CJ, Griffiths JR. The deformation and fracture behaviour of an casting alloy. Mater Sci Eng, A 1995;197(2):171–9.
[5] Zhang Y, Zheng H, Liu Y, Shi L, Xu R, Tian X. Cluster-assisted nucleation of silicon phase in hypoeutectic Al–Si alloy with further inoculation. Acta Mater 2014;70:162–73.
[6] Lu Z, Zhang LJ. Thermodynamic description of the quaternary Al-Si-Mg-Sc system and its application to the design of novel Sc-additional A356 alloys. Mater Des 2017;116:427–37.
[7] Lu S-Z, Hellawell A. The mechanism of silicon modification in aluminum-silicon alloys: impurity induced twinning. Metall Trans A 1987;18(10):1721–33.
[8] Mathiesen RH, Arnberg L, Li Y, Meier V, Schaffer PL, Snigireva I, et al. X-ray videomicroscopy studies of eutectic Al-Si solidification in Al-Si-Cu. Metall Mater Trans 2011;42(1):170–80.
[9] Nabawy AM, Samuel AM, Alkahtani SA, Abuhasel KA, Samuel FH. Role of cerium, lanthanum, and strontium additions in an Al – Si – Mg (A356) alloy. Int J Mater Res 2016;107(5):446–58.
[10] Denton JR, Spittle JA. Solidification and susceptibility to hydrogen absorption of AL–Si alloys containing strontium. Mater Sci Technol 1985;1(4):305–11.
[11] Birol Y. A novel Al–Ti–B alloy for grain refining Al–Si foundry alloys. J Alloys Compd 2009;486(1):219–22.
[12] Birol Y. Impact of grain size on mechanical properties of AlSi7Mg0.3 alloy. Mater Sci Eng, A 2013;559:394–400.
[13] Spittle JA, Sadli S. Effect of alloy variables on grain refinement of binary aluminium alloys with Al–Ti–B. Mater Sci Technol 1995;11(6):533–7.

[14] Zhu M, Yang G, Yao L, Cheng S, Zhou Y. Influence of Al-Ti-B addition on the microstructure and mechanical properties of A356 alloys. Rare Met 2009;28(2):181–6.
[15] Mao G, Tong G, Gao W, Liu S, Zhong L. The poisoning effect of Sc or Zr in grain refinement of Al-Si-Mg alloy with Al-Ti-B. Mater Lett 2021;302:130428.
[16] Luo Q, Li Q, Zhang J-Y, Chen S-L, Chou K-C. Experimental investigation and thermodynamic calculation of the Al–Si–Ti system in Al-rich corner. J Alloys Compd 2014;602:58–65.
[17] Li Y, Gu Q-F, Luo Q, Pang Y, Chen S-L, Chou K-C, et al. Thermodynamic investigation on phase formation in the Al–Si rich region of Al–Si–Ti system. Mater Des 2016;102:78–90.
[18] Li Y, Hu B, Liu B, Nie A, Gu Q, Wang J, et al. Insight into Si poisoning on grain refinement of Al-Si/Al-5Ti-B system. Acta Mater 2020;187:51–65.
[19] Chen XG, Fortier M. Formation of primary TiAlSi intermetallic compounds in Al-Si foundry alloys. Mater Forum 2004;28:659–65.
[20] Spittle JA. Grain refinement in shape casting of aluminium alloys. Int J Cast Metals Res 2006;19(4):210–22.
[21] Samuel AM, Doty HW, Valtierra S, Samuel FH. A metallographic study of grain refining of Sr-modified 356 alloy. Int J Metalcast 2017;11(2):305–20.
[22] Sigworth GK, Kuhn TA. Grain refinement of aluminum casting alloys. Int J Metalcast 2007;1(1):31–40.
[23] Ghomashchi R. The evolution of AlTiSi intermetallic phases in Ti-added A356 Al–Si alloy. J Alloys Compd 2012;537:255–60.
[24] Patakham U, Kajornchaiyakul J, Limmaneevichitr C. Modification mechanism of eutectic silicon in Al–6Si–0.3Mg alloy with scandium. J Alloys Compd 2013;575:273–84.
[25] Pramod SL, Prasada Rao AK, Murty BS, Bakshi SR. Effect of Sc addition on the microstructure and wear properties of A356 alloy and A356–TiB2 in situ composite. Mater Des 2015;78:85–94.
[26] Lu Z, Tang Y, Zhang L. Atomic mobility in liquid and fcc Al–Si–Mg–RE (RE = Ce, Sc) alloys and its application to the simulation of solidification processes in RE-containing A357 alloys. Int J Mater Res 2017;108(6):465–76.
[27] Lu Z, Zhang LJ, Wang J, Yao QR, Rao GH, Zhou HY. Understanding of strengthening and toughening mechanisms for Sc-modified Al-Si-(Mg) series casting alloys designed by computational thermodynamics. J Alloys Compd 2019;805:415–25.
[28] Xu C, Xiao W, Hanada S, Yamagata H, Ma C. The effect of scandium addition on microstructure and mechanical properties of Al–Si–Mg alloy: a multi-refinement modifier. Mater Char 2015;110:160–9.
[29] Pandee P, Gourlay CM, Belyakov SA, Ozaki R, Yasuda H, Limmaneevichitr C. Eutectic morphology of Al-7Si-0.3Mg alloys with scandium additions. Metall Mater Trans 2014;45(10):4549–60.
[30] Prukkanon W, Srisukhumbowornchai N, Limmaneevichitr C. Modification of hypoeutectic Al–Si alloys with scandium. J Alloys Compd 2009;477(1):454–60.
[31] Pramod SL, Ravikirana, Rao AKP, Murty BS, Bakshi SR. Effect of Sc addition and T6 aging treatment on the microstructure modification and mechanical properties of A356 alloy. Mater Sci Eng, A 2016;674:438–50.
[32] Zhang W, Liu Y, Yang J, Dang J, Xu H, Du Z. Effects of Sc content on the microstructure of As-Cast Al-7wt.% Si alloys. Mater Char 2012;66:104–10.
[33] Rajinikanth V, Jindal V, Akkimardi VG, Ghosh M, Venkateswarlu K. Transmission electron microscopy studies on the effect of strain on Al and Al–1% Sc alloy. Scripta Mater 2007;57(5):425–8.
[34] Zakharov VV. Special features of crystallization of scandium-alloyed aluminum alloys. Met Sci Heat Treat 2012;53(9–10):414–9.
[35] Norman AF, Prangnell PB, McEwen RS. The solidification behaviour of dilute aluminium–scandium alloys. Acta Mater 1998;46(16):5715–32.
[36] Hyde KB, Norman AF, Prangnell PB. The effect of cooling rate on the morphology of primary Al3Sc intermetallic particles in Al–Sc alloys. Acta Mater 2001;49(8):1327–37.
[37] Asta M, Foiles SM, Quong A. First-principles calculations of bulk and interfacial thermodynamic properties for fcc-based Al-Sc alloys. Phys Rev B Condens Matter 1998;57:11265–75.
[38] Yan K, Chen ZW, Zhao YN, Ren CC, Lu WJ, Aldeen AW. Morphological characteristics of Al3Sc particles and crystallographic orientation relationships of Al3Sc/Al interface in cast Al-Sc alloy. J Alloys Compd 2021;861.
[39] Patakham U, Kajornchaiyakul J, Limmaneevichitr C. Grain refinement mechanism in an Al–Si–Mg alloy with scandium. J Alloys Compd 2012;542:177–86.
[40] Zhang MX, Kelly PM, Easton MA, Taylor JA. Crystallographic study of grain refinement in aluminum alloys using the edge-to-edge matching model. Acta Mater 2005;53(5):1427–38.
[41] Marquis EA, Seidman DN. Nanoscale structural evolution of Al3Sc precipitates in Al(Sc) alloys. Acta Mater 2001;49(11):1909–19.
[42] Liu S, Wang X, Zu Q, Han B, Han X, Cui C. Significantly improved particle strengthening of Al–Sc alloy by high Sc composition design and rapid solidification. Mater Sci Eng, A 2021;800:140304.
[43] Liu ZW, Cheng N, Zheng QL, Wu JH, Han QY, Huang ZF, et al. Processing and tensile properties of A356 composites containing in situ small-sized Al3Ti particulates. Materials Science and Engineering a-Structural Materials Properties Microstructure and Processing 2018;710:392–9.
[44] Hyde KB, Norman AF, Prangnell PB. The effect of Ti on grain refinement in Al-Sc alloys. Mater Sci Forum 2002;396–402:39–44.
[45] Batsanov SS. The atomic radii of the elements. Russ J Inorg Chem 1991;36:1694–706.
[46] Batsanov SS. Van der Waals radii of elements. Inorg Mater 2001;37(9):871–85.
[47] Du G, Deng J, Wang Y, Yan D, Rong L. Precipitation of (Al,Si)3Sc in an Al–Sc–Si alloy. Scripta Mater 2009;61(5):532–5.
[48] Ludwig TH, Schaffer PL, Arnberg L. Influence of some trace elements on solidification path and microstructure of Al-Si foundry alloys. Metall Mater Trans 2013;44(8):3783–96.
[49] Zuo M, Liu X. Refinement of hypereutectic Al–Si alloy by a new Al–Sc–P master alloy. J Inorg Organomet Polym Mater 2012;22(1):64–9.
[50] Ludwig TH, Li J, Schaffer PL, Schumacher P, Arnberg L. Refinement of eutectic Si in high purity Al-5Si alloys with combined Ca and P additions. Metall Mater Trans 2015;46(1):362–76.
[51] Fang X, Li H, Li X, Huang K, Zhang L, Lu B. Effect of post heat treatment on the microstructure and mechanical properties of wire-arc additively manufactured A357 alloy components. Mater Lett 2020;269:127674.
[52] Lakshmikanthan A, Bontha S, Krishna M, Koppad PG, Ramprabhu T. Microstructure, mechanical and wear properties of the A357 composites reinforced with dual sized SiC particles. J Alloys Compd 2019;786:570–80.